

On the Moment of Inertia of PSR J0737-3039 A from LIGO/Virgo and NICER

ZHIQIANG MIAO¹ AND ANG LI¹

¹*Department of Astronomy, Xiamen University, Xiamen, Fujian 361005, China; liang@xmu.edu.cn*

(Dated: July 19, 2021)

ABSTRACT

We extend our previous study (Li et al. 2021) on neutron stars with a quark core to predict the moment of inertia of pulsar A in the double pulsar binary J0737-3039, assuming there is a phase transition in the pulsar inner core from the soft QMF or the stiff DD2 hadronic equation of state (EOS) to a high-density phase of quark matter modelled by the generic “constant-sound-speed” (CSS) parameterization. We perform a Bayesian analysis of the moment of inertia by incorporating observational data for the tidal deformability of the GW170817 and GW190425 binary neutron star mergers, as detected by LIGO/Virgo, and the mass and radius of PSR J0030+0451 and MSP J0740+6620, as detected by the Neutron Star Interior Composition Explorer. We find that the most probable values of the moment of inertia of PSR J0737-3039 A are $1.27^{+0.18}_{-0.14} \times 10^{45} \text{ g cm}^2$ for QMF+CSS and similarly $1.29^{+0.26}_{-0.15} \times 10^{45} \text{ g cm}^2$ for DD2+CSS at 90% credible interval. We also demonstrate how a moment of inertia measurement would improve our knowledge of the EOS and the mass-radius relation for hybrid stars and discuss whether a quark deconfinement phase transition is supported by the available data and forthcoming data that could be consistent with this hypothesis.

1. INTRODUCTION

Observations of neutron stars (NSs) provide valuable information on the internal structure of these objects and, therefore, on the nuclear equation of state (EOS). Various observables are tightly related with microphysics inside the star and can help to set reliable constraints on it. Among them, there are the mass (Demorest et al. 2010; Antoniadis et al. 2013; Cromartie et al. 2020; Fonseca et al. 2021), the radius (Riley et al. 2019a, 2021a; Miller et al. 2019, 2021), and the tidal deformability (Abbott et al. 2017, 2018). In addition, measurements are planned for the moment of inertia (MOI) of PSR J0737-3039 A (hereafter A) (Lyne et al. 2004), the $1.338 M_{\odot}$ primary component of the first double pulsar system PSR J0737-3039 (Burgay et al. 2003), based on the long-term pulsar timing to determine the periastron advance due to relativistic spin-orbit coupling (Damour & Schafer 1988). The MOI of A is expected to be measured with $\sim 10\%$ accuracy within the next decade (Hu et al. 2020), which will provide complementary constraints on the EOS.

The NS MOI has been theoretically calculated using a wide range of EOS models (e.g., Yuan & Zhang 1999; Morrison et al. 2004; Lattimer & Schutz 2005; Bejger et al. 2005; Rikowska Stone et al. 2007; Klähn et al. 2007;

Read et al. 2009; Urbanec et al. 2013; Motta et al. 2019; Sun et al. 2019; Wei et al. 2019; Lourenço et al. 2020; Margaritis et al. 2020). Several studies have been performed using EOS models, including those incorporating strangeness phase transitions (e.g., Klähn et al. 2007; Bandyopadhyay et al. 2018; Sen & Jha 2019; Ribes et al. 2019; Fortin et al. 2020; Raduta et al. 2020).

In several recent studies, the MOI of A has been predicted based on EOSs constrained using physical stability arguments (Raithel et al. 2016), NS observations (Steiner et al. 2015; Landry & Kumar 2018; Kumar & Landry 2019; Jiang et al. 2020; Silva et al. 2021), or the results of nuclear experiments (Worley et al. 2008; Lim et al. 2019). However, a phase transition was not explicitly taken into account in these previous studies. Although the occurrence of a phase transition in NS cores remains a subject of debate, EOSs with an early phase transition at $\sim 2n_0$ (where $n_0 = 0.16 \text{ fm}^{-3}$ denotes the nuclear saturation density) are compatible with current NS observations (Al-Mamun et al. 2021; Li et al. 2020, 2021; Miao et al. 2020; Xie & Li 2021). Therefore, there is a possibility that A is a hybrid star with a substantial quark matter core (Li et al. 2021).

In the present study, within the context of a first-order phase transition from hadronic matter to quark matter in the NS interior, we make a direct estimate of

the MOI of A based on a Bayesian analysis of available gravitational-wave data from LIGO/Virgo and mass-radius measurements from the Neutron Star Interior Composition Explorer (*NICER*). For our purpose, we focus on the EOS flexibility in the quark matter phase, for which we employ a “constant-speed-of-sound” (CSS) parameterization (Alford et al. 2013), while utilizing two representative hadronic EOSs (Zhu et al. 2018; Fortin et al. 2016) to test the effect of low-density hadronic matter.

This paper is organized as follows. In Section 2, we introduce the EOSs used to model the hadronic phase of NSs and the CSS parameterization for describing the phase transition and the quark matter phase of NSs. The NS observations used and the Bayesian analysis method are detailed in Section 3. We present our results and a discussion in Section 4 and summarize our paper in Section 5.

2. NSS WITH OR WITHOUT A QUARK CORE

Following our previous study (Li et al. 2021), we describe NSs with and without a quark core below.

For NSs without a quark core, we employ the unified QMF (Zhu et al. 2018) and DD2 (Fortin et al. 2016) EOS models for soft and stiff hadronic matter, while using the standard BPS EOS for the NS outer crust (Baym et al. 1971). Solving the Tolman-Oppenheimer-Volkoff (TOV) equations yields the NS maximum mass as $M_{\text{TOV}}^{\text{QMF}} = 2.07 M_{\odot}$ and $M_{\text{TOV}}^{\text{DD2}} = 2.42 M_{\odot}$, with the radius of a typical $1.4 M_{\odot}$ star as $R_{1.4}^{\text{QMF}} = 11.77 \text{ km}$ and $R_{1.4}^{\text{DD2}} = 13.17 \text{ km}$, respectively. Furthermore, as the rotation frequency of A, $\Omega_A = 276.8 \text{ Hz}$ (Burgay et al. 2003) is far smaller than the Kepler frequency, one can employ the slow rotation approximation (Hartle 1967) to calculate the MOI of A, which is $I_A^{\text{QMF}} = 1.33 \times 10^{45} \text{ g cm}^2$ and $I_A^{\text{DD2}} = 1.60 \times 10^{45} \text{ g cm}^2$ using the two EOSs.

For NSs with a quark core, we implement a sharp first-order phase transition between the hadronic and quark phases by employing the CSS parameterization (Alford et al. 2013), while maintaining the hadronic EOS as QMF or DD2. The full EOS can be expressed as follows (we use units where $\hbar = c = 1$):

$$\varepsilon(p) = \begin{cases} \varepsilon_{\text{HM}}(p), & p < p_{\text{trans}} \\ \varepsilon_{\text{HM}}(p_{\text{trans}}) + \Delta\varepsilon + c_{\text{QM}}^{-2}(p - p_{\text{trans}}), & p > p_{\text{trans}} \end{cases} \quad (1)$$

where p_{trans} is the pressure of the transition, $\Delta\varepsilon$ is the discontinuity in the energy density, and c_{QM} is the sound speed in quark matter. Correspondingly, three dimensionless parameters are chosen as the EOS parameters of hybrid stars, namely, the transition density n_{trans}/n_0 , the transition strength $\Delta\varepsilon/\varepsilon_{\text{trans}}$, and

the sound speed squared in quark matter c_{QM}^2 , where $n_{\text{trans}} \equiv n_{\text{HM}}(p_{\text{trans}})$ and $\varepsilon_{\text{trans}} \equiv \varepsilon_{\text{HM}}(p_{\text{trans}})$.

The EOS parameters are varied to obtain a 3D parameter space for the EOSs, and a Bayesian analysis is performed to select preferred EOSs based on NS observations. The Bayesian analysis framework is introduced in the next section.

3. OBSERVATIONAL CONSTRAINTS AND BAYESIAN ANALYSIS

In the present study, our observational data set \mathbf{d} contains two gravitational wave events (GW170817 and GW190425) and two *NICER* mass-radius measurements of pulsars (PSR J0030+0451 and MSP J0740+6620). First, we begin with the likelihood of reproducing the data using the EOS model with the parameter set θ . The likelihood can be expressed as

$$\mathcal{L}(\mathbf{d}|\theta, \mathbf{p}_c) = \prod_i \mathcal{L}_{\text{GW},i} \times \prod_j \mathcal{L}_{\text{NICER},j} \quad (2)$$

where \mathbf{p}_c is the central pressure of the *NICER*’s pulsars (see more discussions in e.g., Li et al. 2021).

GW170817 and GW190425. We treat both GW170817 and GW190425 as binary NS mergers. We calculate the likelihood of each gravitational event through a high-precision interpolation of the likelihood developed in Hernandez Vivanco et al. (2020), which is encapsulated in the python package *toast*, i.e.,

$$\mathcal{L}_{\text{GW},i} = F_i(\Lambda_1, \Lambda_2, \mathcal{M}_c, q) \quad (3)$$

where $F_i(\cdot)$ is the interpolation function of the gravitational wave event i . The chirp mass $\mathcal{M}_c \equiv (M_1 M_2)^{3/5} / (M_1 + M_2)^{1/5}$ and the mass ratio $q \equiv M_2 / M_1$. The tidal deformabilities can be derived from the component masses, i.e., $\Lambda_1 = \Lambda_1(\theta; M_1)$ and $\Lambda_2 = \Lambda_2(\theta; M_2)$.

***NICER* mass-radius measurements** Recently, the *NICER* collaboration reported simultaneous mass-radius measurements of PSR J0030+0451 and MSP J0740+6620. The results for PSR J0030+0451 were $M = 1.34^{+0.15}_{-0.16} M_{\odot}$, $R = 12.71^{+1.14}_{-1.19} \text{ km}$ (Riley et al. 2019a) or $M = 1.44^{+0.15}_{-0.14} M_{\odot}$, $R = 13.02^{+1.24}_{-1.06} \text{ km}$ (Miller et al. 2019). The results for MSP J0740+6620 were $M = 2.072^{+0.067}_{-0.066} M_{\odot}$, $R = 12.39^{+1.30}_{-0.98} \text{ km}$ (Riley et al. 2021a) or $M = 2.062^{+0.090}_{-0.091} M_{\odot}$, $R = 13.71^{+2.61}_{-1.50} \text{ km}$ (Miller et al. 2021). To incorporate each of these measurements, we write the likelihood as

$$\mathcal{L}_{\text{NICER},j} = \text{KDE}(M, R|\mathbf{S}_j) \quad (4)$$

where the right-hand side is a kernel density estimation of the posterior samples \mathbf{S}_j of the mass-radius measurement j . Similar to Li et al. (2021), we use the

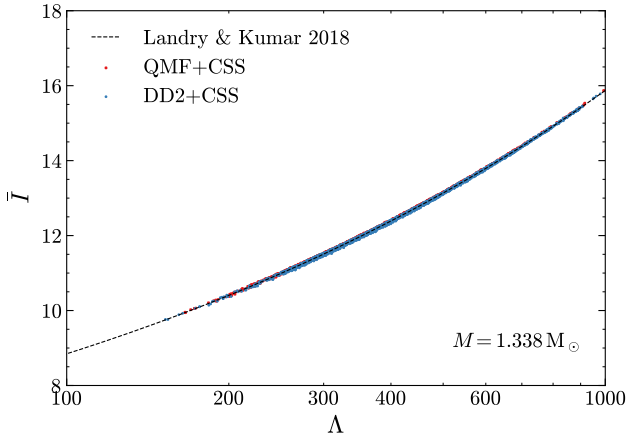


Figure 1. Posterior distribution of $\bar{I} \equiv I/M^3$ vs. Λ for a $1.338 M_\odot$ star, transformed from the EOS parameter posteriors. The black dashed line shows the fitting formula from Landry & Kumar (2018), updated from the original relation of Yagi & Yunes (2013) with a larger set of EOSs.

ST+PST model samples from Riley et al. (2019b) for PSR J0030+0451. For MSP J0740+6620, we use the *NICER* \times XMM samples from Riley et al. (2021b). The mass and radius (M, R) are mapped from the EOS parameters θ and the central pressure p_c through the TOV equations.

To recap, we consider two families of EOS models in the present analysis, namely, QMF+CSS and DD2+CSS, as detailed in Section 2. The EOS parameters are $\theta = \{n_{\text{trans}}/n_0, \Delta\varepsilon/\varepsilon_{\text{trans}}, c_{\text{QM}}^2\}$, for which we employ the priors used in our previous study (Li et al. 2021).

4. RESULTS AND DISCUSSION

In this section, we use the nested sampling software PyMultiNest (Buchner et al. 2014) to generate posterior samples for analyzing the NS properties. We obtain a total of approximately 3,000 posterior samples of the CSS model parameters for both QMF+CSS and DD2+CSS.

4.1. MOI of PSR J0737-3039 A

Fig. 1 presents the posterior distributions of the dimensionless MOI $\bar{I} \equiv I/M^3$ vs. the tidal deformability Λ . The analysis is performed for a fixed star mass $M = 1.338 M_\odot$, corresponding to A. Our results can be effectively reconciled with the universal relation of NSs (shown as a black line in Fig. 1) (Yagi & Yunes 2013; Landry & Kumar 2018), with an error less than 0.5%, indicating that the I-Love relation remains valid within the present hybrid star scenario (see also in, e.g., Miao et al. 2020).

In Fig. 2, we show the 90% bounds on the MOI for A as a function of the A radius. Also shown is the extreme bound from Raithel et al. (2016), which is derived by

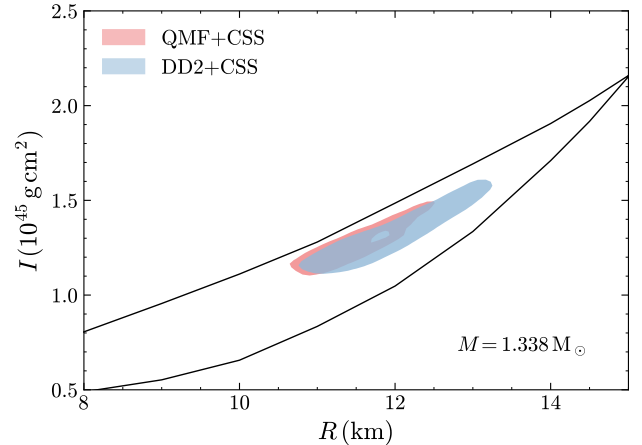


Figure 2. Theoretical bounds on the MOI of J0737-3039 A as a function of its radius, within both QMF+CSS and DD2+CSS (90% credible interval). The black curve corresponds to an extreme bound from Raithel et al. (2016), assuming the AP4 EOS up to nuclear saturation density n_0 and a constant-density core inside the NSs.

Table 1. Theoretical predictions on the MOI of J0737-3039 A ($M = 1.338 M_\odot$). Except the values of Worley et al. (2008), the quoted error bars refer to symmetric 90% credible intervals about the median. The MOI are given in 10^{45} g cm^2 .

Reference	I_A
Worley et al. (2008)	[1.30, 1.63]
Landry & Kumar (2018)	$1.15^{+0.38}_{-0.24}$
Lim et al. (2019)	$1.36^{+0.12}_{-0.26}$
Jiang et al. (2020)	$1.35^{+0.26}_{-0.14}$
Silva et al. (2021)	$1.68^{+0.53}_{-0.48}$
This work (QMF+CSS)	$1.27^{+0.18}_{-0.14}$
This work (DD2+CSS)	$1.29^{+0.26}_{-0.15}$

placing one or two constant-density cores inside the NSs based on stability arguments, whereas the outer layer (with a density lower than the nuclear saturation density) is described by the AP4 EOS. The EOS modelling results based on currently available NS observations fall within a fairly narrow region of the $I - R$ plane.

In Table 1, we compare our MOI prediction for A with those of previous studies. Using EOS-insensitive relations, Landry & Kumar (2018) resulted in an MOI of $\sim 1.15 \times 10^{45} \text{ g cm}^2$ based on the GW170817 tidal measurement. In Silva et al. (2021), a larger MOI of $\sim 1.68 \times 10^{45} \text{ g cm}^2$ was obtained based on the *NICER* mass-radius measurement of PSR J0030+0451 at 90% credible interval. In Jiang et al. (2020), both data sets were used with parameterized EOSs to obtain an MOI between

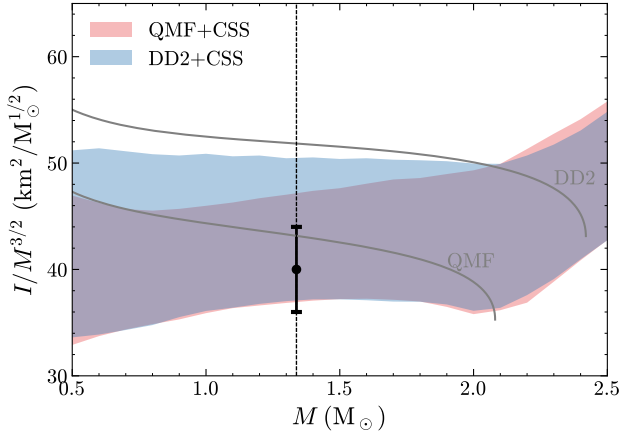


Figure 3. The 90% credible regions of $I/M^{3/2}$ as a function of M , transformed from the EOS parameter posteriors. Also shown in solid grey lines are the results of two NS EOSs (QMF and DD2). The vertical line corresponds to $M = 1.338 M_\odot$, while the error bar represents a hypothetical 10% precision measurement centered on $I/M_A^{3/2} = 40 \text{ km}^2/M_\odot^{1/2}$.

$\sim 1.35 \times 10^{45} \text{ g cm}^2$. In the present study, we not only explicitly include the possibility of a phase transition in the EOS prior but also incorporate two additional sources, GW190425 and MSP J0740+6620, into the analysis. Our results indicate that $I_{1.338} = 1.27^{+0.18}_{-0.14} \times 10^{45} \text{ g cm}^2$ (or $I/M_A^{3/2} = 41.3^{+5.8}_{-4.5} \text{ km}^2/M_\odot^{1/2}$) within QMF+CSS or $1.29^{+0.26}_{-0.15} \times 10^{45} \text{ g cm}^2$ (or $I/M_A^{3/2} = 41.9^{+8.4}_{-4.9} \text{ km}^2/M_\odot^{1/2}$) within DD2+CSS at 90% credible interval. Predictions have also been made based on EOSs constrained by relativistic heavy-ion collisions (Worley et al. 2008) or microscopic EOSs consistent with empirical data for finite nuclei (Lim et al. 2019), as shown in Table 1.

For subsequent calculations, Fig 3 shows the posterior distributions of $I/M^{3/2}$ as a function of the mass M . The scaled MOI is found to lie within the range $I/M^{3/2} \sim 35 - 50 \text{ km}^2/M_\odot^{1/2}$. Note that in Steiner et al. (2015), a similar and somewhat narrower range of $\sim 35 - 45 \text{ km}^2/M_\odot^{1/2}$ was calculated based on two sets of parameterized EOSs (which were denoted as Models A and C) obtained from analyzing several mass-radius measurements from photospheric radius expansion (PRE) bursts or quiescent low-mass X-ray binaries.

Below, we use the implications of the LIGO/Virgo and NICER data for the MOI of A (as shown in Fig. 3) to analyze mocked data consisting of a future MOI measurement of A with an accuracy of 10%. In Sec. 4.2, we present updated constraints on the EOS of NS matter and the corresponding mass-radius relations of the stars. In Sec. 4.3, we evaluate in detail whether a phase transition is supported by current and future observational data.

4.2. Updated constraints with mocked MOI measurements of PSR J0737-3039 A

The MOI of A is expected to be measured with 11 percent precision at a 68% confidence level in 2030 (Hu et al. 2020), and the results will provide further constraints on the EOS and NS properties. To determine how such a precise MOI measurement would improve our present knowledge of the mass-radius relation, we carry out four tests (Tests i-iv) incorporating mocked data for future measurements of the MOI for A into our Bayesian analysis framework.

For Test i to Test iv, we add MOI measurements scaled by $M_A^{3/2}$ as $I/M_A^{3/2} = 35, 40, 45, 50 \text{ km}^2/M_\odot^{1/2}$, with a 10% accuracy for all four cases. We repeat the sampling process for the NSs and report the results in Table 2, that is, the sound speed squared in quark matter c_{QM}^2 , the maximum mass M_{TOV} and the radius of a typical $1.4 M_\odot$ star $R_{1.4}$ for hybrid stars, along with results from Li et al. (2021). The 90% credible regions of the EOSs are shown in Fig. 4 with and without the mocked MOI measurement for the representative QMF+CSS case. Fig. 5 shows the corresponding results for the mass-radius relations.

We found in Li et al. (2021) that the maximum mass of NSs is $M_{\text{TOV}} = 2.36^{+0.49}_{-0.26} M_\odot$ ($2.39^{+0.42}_{-0.28} M_\odot$) and the radius of a $1.4 M_\odot$ star is $R_{1.4} = 11.70^{+0.85}_{-0.74} \text{ km}$ ($11.95^{+1.04}_{-0.94} \text{ km}$) at 90% credible interval for QMF+CSS (DD2+CSS) by incorporating both the GW170817 data and the NICER mass-radius measurement of PSR J0030+0451, as well as the $2.14 M_\odot$ mass measurement of MSP J0740+6620 from radio timing. In the present study, the peak value of the maximum mass shifts from $\sim 2.4 M_\odot$ to $\sim 2.2 M_\odot$ by updating the MSP J0740+6620 data with a more restrictive mass-radius measurement from the NICER x XMM data¹, indicating that a softer EOS is required. This result can also be directly inferred from the posterior distribution of the sound speed squared in quark matter c_{QM}^2 , whose median shifts from ~ 0.8 to ~ 0.7 . As the resulting maximum mass is insensitive to the hadronic EOS (Li et al. 2021), we employ a weighted average of the combined posteriors and find $M_{\text{TOV}} = 2.23^{+0.41}_{-0.21} M_\odot$ at 90%

¹ Apart from updating the MSP J0740+6620 data, there are two other differences between this study and Li et al. (2021): 1) the likelihood of encapsulating gravitational wave data obtained using the interpolation function and 2) additional GW190425 data. For the former, we checked that the results obtained using the interpolation function are consistent with those obtained using gravitational wave data, whereas for the latter, we proved that the addition of GW190425 data had a small effect on the results. Therefore, we consider the main difference between this study and Li et al. (2021) to be the MSP J0740+6620 data update.

Table 2. The resulting sound speed squared in quark matter c_{QM}^2 , the maximum mass M_{TOV} and the radius of a $1.4 M_{\odot}$ star $R_{1.4}$ are collected for both cases of QMF+CSS and DD2+CSS, from our previous work (Li et al. 2021) (in the 2nd column) and the present work (in the 3rd column). In the last four columns, we show the results of four tests when a mocked MOI measurement is added, being $I/M_{\text{A}}^{3/2} = 35, 40, 45, 50 \text{ km}^2/M_{\odot}^{1/2}$, respectively. The quoted error bars refer to symmetric 90% credible intervals about the median. The Bayes factors of the hybrid star against the normal NS, $\mathcal{B}_{\text{NS}}^{\text{HS}}$, are also shown for each case. See text for details.

	GW170817+ PSR J0030 (Li et al. 2021)	GW170817+GW190425 +PSR J0030+ PSR J0740	+Mocked MOI measurement			
			Test i	Test ii	Test iii	Test iv
QMF+CSS						
c_{QM}^2	$0.81^{+0.17}_{-0.28}$	$0.73^{+0.24}_{-0.30}$	$0.77^{+0.21}_{-0.27}$	$0.74^{+0.24}_{-0.27}$	$0.71^{+0.26}_{-0.28}$	$0.70^{+0.27}_{-0.30}$
M_{TOV}/M_{\odot}	$2.36^{+0.49}_{-0.26}$	$2.23^{+0.42}_{-0.21}$	$2.22^{+0.29}_{-0.20}$	$2.24^{+0.35}_{-0.22}$	$2.23^{+0.44}_{-0.22}$	$2.25^{+0.54}_{-0.24}$
$R_{1.4}/\text{km}$	$11.70^{+0.85}_{-0.74}$	$11.61^{+0.75}_{-0.76}$	$11.21^{+0.60}_{-0.60}$	$11.52^{+0.48}_{-0.67}$	$11.74^{+0.60}_{-0.68}$	$11.88^{+0.75}_{-0.61}$
$\mathcal{B}_{\text{NS}}^{\text{HS}}$	1.49	0.63	1.77	0.66	0.43	0.44
DD2+CSS						
c_{QM}^2	$0.80^{+0.18}_{-0.29}$	$0.71^{+0.26}_{-0.29}$	$0.78^{+0.20}_{-0.26}$	$0.73^{+0.25}_{-0.27}$	$0.69^{+0.27}_{-0.28}$	$0.68^{+0.29}_{-0.28}$
M_{TOV}/M_{\odot}	$2.39^{+0.42}_{-0.28}$	$2.23^{+0.39}_{-0.21}$	$2.23^{+0.27}_{-0.21}$	$2.25^{+0.35}_{-0.22}$	$2.25^{+0.41}_{-0.22}$	$2.22^{+0.45}_{-0.20}$
$R_{1.4}/\text{km}$	$11.95^{+1.04}_{-0.94}$	$11.89^{+1.15}_{-0.93}$	$11.28^{+0.59}_{-0.62}$	$11.60^{+0.81}_{-0.68}$	$12.06^{+0.89}_{-0.84}$	$12.51^{+0.65}_{-0.99}$
$\mathcal{B}_{\text{NS}}^{\text{HS}}$	1.78	2.80	4.48×10^4	95.20	3.72	1.40

credible interval. There is also a slight decrease in the radius due to this update. The inferred radius changes from $11.70^{+0.85}_{-0.74} \text{ km}$ ($11.95^{+1.04}_{-0.94} \text{ km}$) to $11.61^{+0.75}_{-0.76} \text{ km}$ ($11.89^{+1.15}_{-0.93} \text{ km}$) for QMF+CSS (DD2+CSS) at 90% credible interval.

Next, we determine the effects of incorporating a mocked MOI measurement into the data. Fig. 4 shows that the additional MOI measurement provides further constraints on the EOS. These constraints on the EOS mainly occur at intermediate densities $\sim 300 - 600 \text{ MeV/fm}^3$ (or equivalently, $\sim 2 - 4 \varepsilon_0$, where $\varepsilon_0 \approx 157 \text{ MeV/fm}^3$ is the nuclear saturation mass density). Note that the results for the Test ii case is close to the most probable value obtained from the present analysis ($I/M_{\text{A}}^{3/2} \sim 41 \text{ km}^2/M_{\odot}^{1/2}$), as reported earlier in Sec. 4.1. In Miller et al. (2020), a MOI measurement with 10% precision close to the favoured value was shown to significantly improve the estimates of the radii for NSs with masses of $M = 1.8 - 2 M_{\odot}$ but had a negligible effect on the corresponding estimates for masses of approximately $M = 1 M_{\odot}$. This result is consistent with our results for the Test ii case (shown in the upper right panel of Fig. 5). The results of the other three tests based on different MOI measurements show that it is possible to improve our estimates of NS radii over the entire mass span.

Additionally, as detailed in Table 2, as the measured MOI increases, the inferred sound speed in quark matter decreases. Taking the QMF+CSS case as

an example, c_{QM}^2 drops from $0.77^{+0.21}_{-0.27}$ at $I/M_{\text{A}}^{3/2} = 35 \text{ km}^2/M_{\odot}^{1/2}$ (Test i) to $0.70^{+0.27}_{-0.30}$ for a measured $I/M_{\text{A}}^{3/2} = 50 \text{ km}^2/M_{\odot}^{1/2}$ (Test iv) because larger stellar radii have softer quark matter EOS (i.e., smaller sound speeds). Finally, it is important to note that the MOI measurement has a limited effect on the resulting maximum mass. The inferred maximum mass is found to be insensitive to the MOI measurement, with the most likely value of the maximum mass remaining at $\sim 2.2 M_{\odot}$.

4.3. With or without deconfined quarks?

In this section, we analyze whether the current data favour a strong first-order phase transition inside NS inner cores. For this purpose, we compute the Bayes factor between the EOS models with and without a phase transition. The results are reported in the sixth and twelfth rows of Table 2.

In general, the Bayes evidences are comparable for both soft QMF and stiff DD2 cases with $|\log(\mathcal{B}_{\text{NS}}^{\text{HS}})| \lesssim 1$, indicating that the current data are compatible with the possibility of a phase transition, namely the compact objects are likely hybrid stars, besides the pure hadronic nature as commonly assumed.

Our results are also slightly dependent on the two hadronic EOSs employed. For instance, by incorporating the J0740 mass-radius measurement into the data, the evidence of a phase transition is slightly enhanced

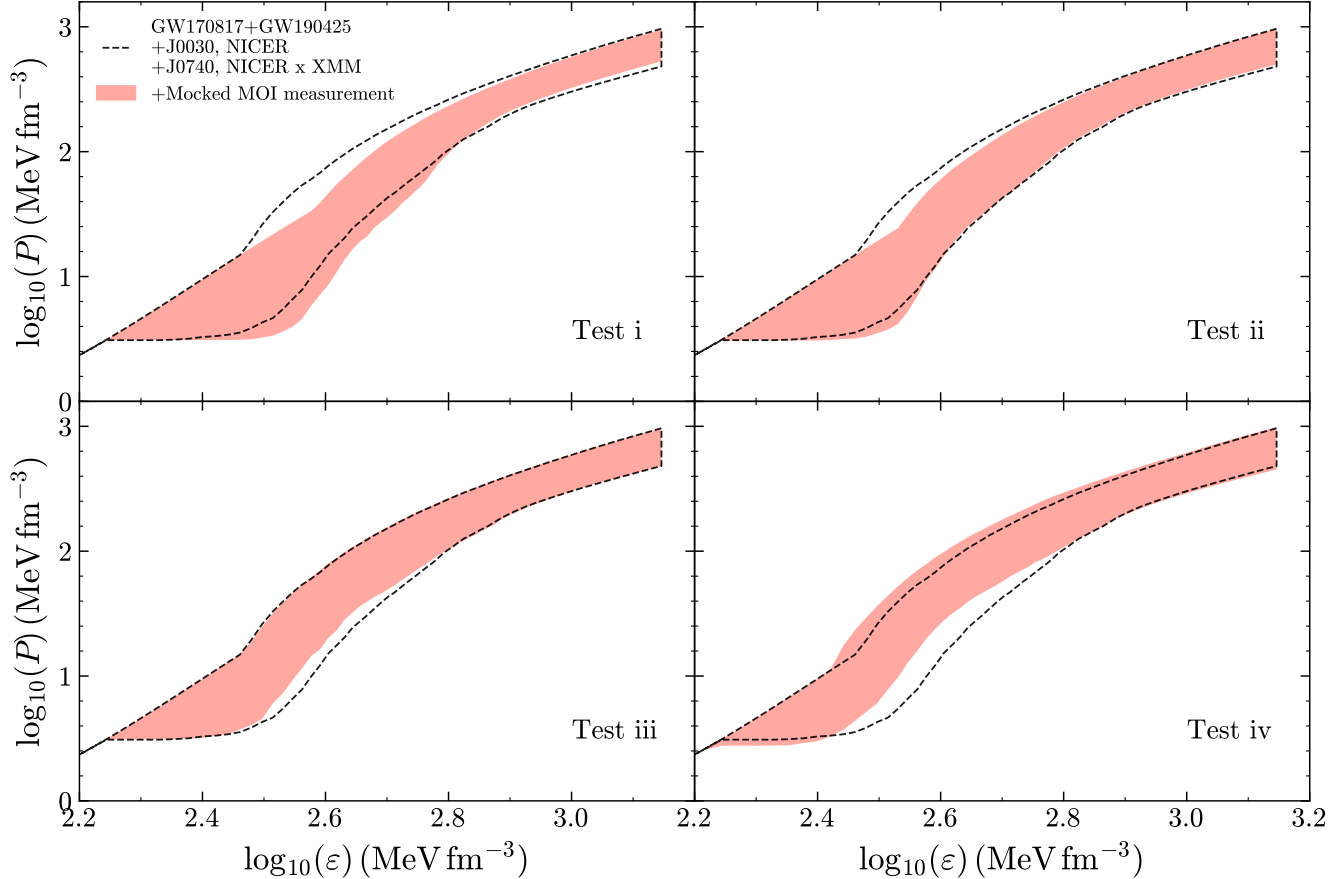


Figure 4. The 90% credible regions of the EOSs for QMF+CSS. The dashed lines show the results from joint analysis of the present data, including two gravitational wave data and two *NICER*’s mass-radius measurements. The red shaded regions show the updated posterior distributions from four tests (i-iv), in which we add a mocked MOI measurement for PSR J0737-3039 A to be $I/M_A^{3/2} = 35, 40, 45, 50 \text{ km}^2 / M_\odot^{1/2}$, respectively.

for the DD2 case ($\mathcal{B}_{\text{NS}}^{\text{HS}}$ increases from 1.78 to 2.80) but slightly weakened for the QMF case ($\mathcal{B}_{\text{NS}}^{\text{HS}}$ decreases from 1.49 to 0.63). The evidence of a phase transition for the DD2 case is strengthened if we include the MOI measurement in the data: Table 2 shows the large Bayes factors, especially for relatively low MOI measurements. Note that the recent PREX-II measurement of the neutron skin of ^{208}Pb indicates a rather stiff symmetry energy (Reed et al. 2021), resulting in a large predicted radius for a $1.4 M_\odot$ star, which may conflict with the tidal deformability constraint from GW170817 (Abbott et al. 2018). An early phase transition, e.g., at $\sim 2n_0$ (Li et al. 2021), could resolve this conflict, because the transition could lead to a lower radius from the softening of the EOS at high densities. Supporting evidence for a phase transition also justifies our introduction of a quark core into the present analysis

5. SUMMARY AND CONCLUSIONS

There is a high expectation of an imminent precise measurement of the NS MOI for the very first time for

the first double pulsar system PSR J0737-3039. Continuing efforts are being made to theoretically predict the MOI of PSR J0737-3039 A based on many modern nuclear EOSs within the constraints provided by the results of nuclear experiments and astrophysical observations. Considering that the pulsar interior may have a quark matter core, it is meaningful to update the MOI analysis of previous studies by incorporating strangeness phase transitions. Furthermore, such an MOI measurement would place new constraints on the NS EOS. A question that naturally follows is what information this measurement will contribute to our understanding of dense matter.

In this study, a hadron-quark phase transition in the EOS prior modelled by the generic CSS parameterization is explicitly considered and a Bayesian analysis is performed on the MOI of PSR J0737-3039 A using available data from LIGO/Virgo and *NICER*. Both soft QMF and stiff DD2 are applied for the low-density hadronic phase to test the model-dependence of the MOI prediction. An MOI of $1.27^{+0.18}_{-0.14} \times 10^{45} \text{ g cm}^2$

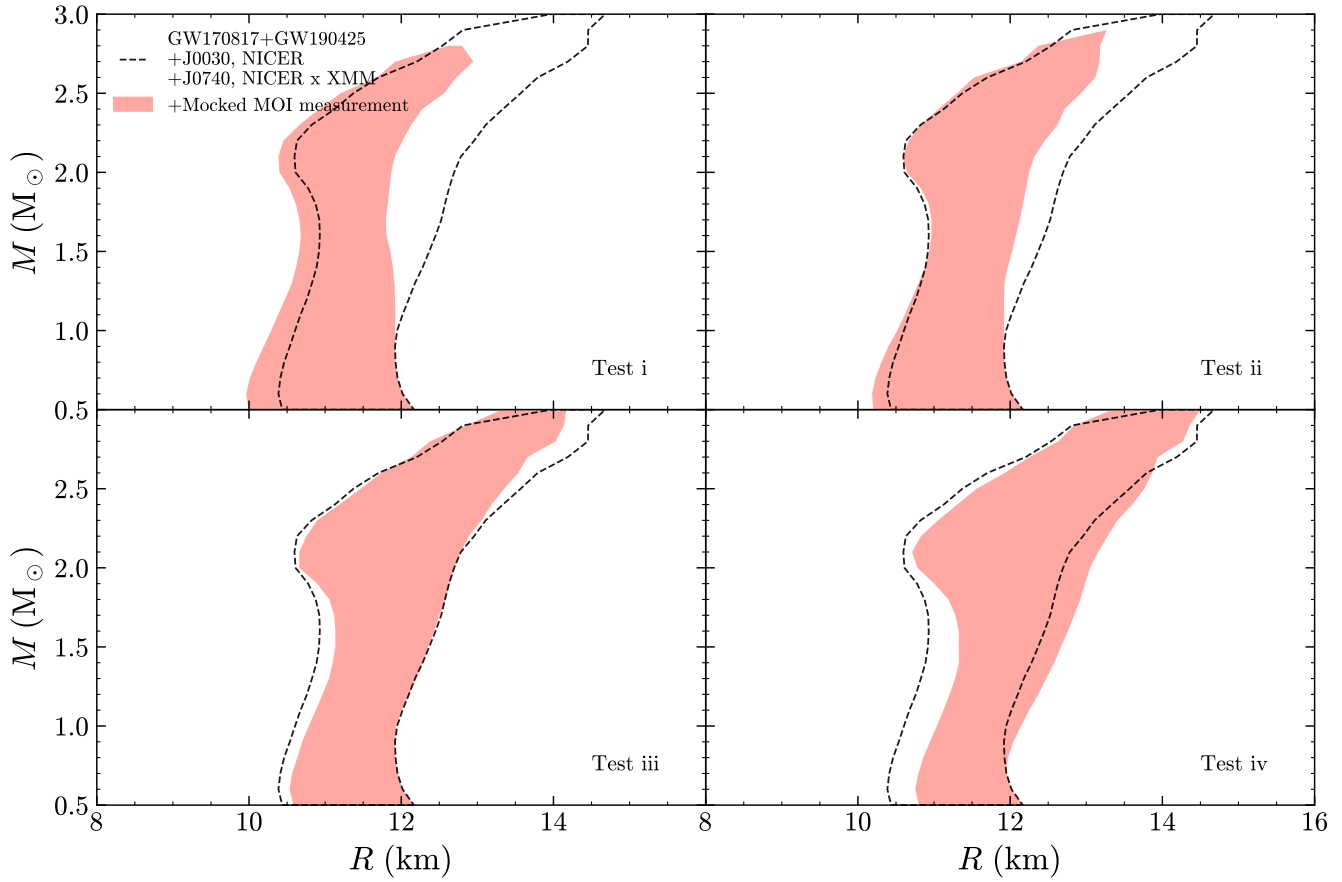


Figure 5. Same as Fig.4, but for the mass-radius relations.

is obtained using QMF+CSS, and a similar result of $1.29^{+0.26}_{-0.15} \times 10^{45} \text{ g cm}^2$ is obtained using DD2+CSS. We also demonstrated in detail that an MOI measurement, when available, can significantly reduce the EOS uncertainties, especially when the MOI value is a few times the nuclear saturation density. In addition, we evaluated the relative probability of a phase transition occurring using the pure hadronic star as a reference state, based on the available data and a potential MOI constraint. The results show that the hybrid star scenario is justified as one of the many possibilities of the nature of pulsars.

ACKNOWLEDGMENTS

We are thankful to Prof. B.-A. Li for helpful discussions. The work is supported by National SKA Program of China (No. 2020SKA0120300), the National Natural Science Foundation of China (Grant No. 11873040), the science research grants from the China Manned Space Project (No. CMS-CSST-2021-B11) and the Youth Innovation Fund of Xiamen (No. 3502Z20206061).

Software: PyMultiNest (Buchner 2016, version 2.6, ascl:1606.005, <https://github.com/JohannesBuchner/PyMultiNest>).

REFERENCES

- Abbott, B. P., Abbott, R., Abbott, T. D., et al. 2017, *PhRvL*, 119, 161101.
doi:10.1103/PhysRevLett.119.161101
- Abbott, B. P., Abbott, R., Abbott, T. D., et al. 2018, *PhRvL*, 121, 161101.
doi:10.1103/PhysRevLett.121.161101
- Al-Mamun, M., Steiner, A. W., Nättilä, J., et al. 2021, *PhRvL*, 126, 061101.
doi:10.1103/PhysRevLett.126.061101
- Alford, M. G., Han, S., & Prakash, M. 2013, *PhRvD*, 88, 083013. doi:10.1103/PhysRevD.88.083013
- Antoniadis, J., Freire, P. C. C., Wex, N., et al. 2013, *Science*, 340, 448. doi:10.1126/science.1233232

- Bandyopadhyay, D., Bhat, S. A., Char, P., et al. 2018, *European Physical Journal A*, 54, 26.
doi:10.1140/epja/i2018-12456-y
- Baym, G., Pethick, C., & Sutherland, P. 1971, *ApJ*, 170, 299. doi:10.1086/151216
- Bejger, M., Bulik, T., & Haensel, P. 2005, *MNRAS*, 364, 635. doi:10.1111/j.1365-2966.2005.09575.x
- Buchner, J. 2016, *Astrophysics Source Code Library*.
ascl:1606.005
- Buchner, J., Georgakakis, A., Nandra, K., et al. 2014, *A&A*, 564, A125. doi:10.1051/0004-6361/201322971
- Burgay, M., D’Amico, N., Possenti, A., et al. 2003, *Nature*, 426, 531. doi:10.1038/nature02124
- Cromartie, H. T., Fonseca, E., Ransom, S. M., et al. 2020, *Nature Astronomy*, 4, 72. doi:10.1038/s41550-019-0880-2
- Damour, T. & Schafer, G. 1988, *Nuovo Cimento B Serie*, 101B, 127. doi:10.1007/BF02828697
- Demorest, P. B., Pennucci, T., Ransom, S. M., et al. 2010, *Nature*, 467, 1081. doi:10.1038/nature09466
- Fonseca, E., Cromartie, H. T., Pennucci, T. T., et al. 2021, *ApJL*, 915, L12. doi:10.3847/2041-8213/ac03b8
- Fortin, M., Providência, C., Raduta, A. R., et al. 2016, *PhRvC*, 94, 035804. doi:10.1103/PhysRevC.94.035804
- Fortin, M., Raduta, A. R., Avancini, S., et al. 2020, *PhRvD*, 101, 034017. doi:10.1103/PhysRevD.101.034017
- Hartle, J. B. 1967, *ApJ*, 150, 1005. doi:10.1086/149400
- Hernandez Vivanco, F., Smith, R., Thrane, E., et al. 2020, *MNRAS*, 499, 5972. doi:10.1093/mnras/staa3243
- Hu, H., Kramer, M., Wex, N., et al. 2020, *MNRAS*, 497, 3118. doi:10.1093/mnras/staa2107
- Jiang, J.-L., Tang, S.-P., Wang, Y.-Z., et al. 2020, *ApJ*, 892, 55. doi:10.3847/1538-4357/ab77cf
- Klähn, T., Blaschke, D., Sandin, F., et al. 2007, *Physics Letters B*, 654, 170. doi:10.1016/j.physletb.2007.08.048
- Kumar, B. & Landry, P. 2019, *PhRvD*, 99, 123026.
doi:10.1103/PhysRevD.99.123026
- Landry, P. & Kumar, B. 2018, *ApJL*, 868, L22.
doi:10.3847/2041-8213/aace76
- Lattimer, J. M. & Schutz, B. F. 2005, *ApJ*, 629, 979.
doi:10.1086/431543
- Li, A., Zhu, Z.-Y., Zhou, E.-P., et al. 2020, *Journal of High Energy Astrophysics*, 28, 19.
doi:10.1016/j.jheap.2020.07.001
- Li, A., Miao, Z., Han, S., et al. 2021, *ApJ*, 913, 27.
doi:10.3847/1538-4357/abf355
- Lim, Y., Holt, J. W., & Stahulak, R. J. 2019, *PhRvC*, 100, 035802. doi:10.1103/PhysRevC.100.035802
- Lourengo, O., Dutra, M., Lenzi, C. H., et al. 2020, *European Physical Journal A*, 56, 32.
doi:10.1140/epja/s10050-020-00040-z
- Lyne, A. G., Burgay, M., Kramer, M., et al. 2004, *Science*, 303, 1153. doi:10.1126/science.1094645
- Margaritis, C., Koliogiannis, P. S., & Moustakidis, C. C. 2020, *PhRvD*, 101, 043023.
doi:10.1103/PhysRevD.101.043023
- Miao, Z., Li, A., Zhu, Z., et al. 2020, *ApJ*, 904, 103.
doi:10.3847/1538-4357/abbd41
- Miller, M. C., Lamb, F. K., Dittmann, A. J., et al. 2021, *arXiv:2105.06979*
- Miller, M. C., Chirenti, C., & Lamb, F. K. 2020, *ApJ*, 888, 12. doi:10.3847/1538-4357/ab4ef9
- Miller, M. C., Lamb, F. K., Dittmann, A. J., et al. 2019, *ApJL*, 887, L24. doi:10.3847/2041-8213/ab50c5
- Morrison, I. A., Baumgarte, T. W., Shapiro, S. L., et al. 2004, *ApJL*, 617, L135. doi:10.1086/427235
- Motta, T. F., Kalaitzis, A. M., Antić, S., et al. 2019, *ApJ*, 878, 159. doi:10.3847/1538-4357/ab218e
- Raduta, A. R., Oertel, M., & Sedrakian, A. 2020, *MNRAS*, 499, 914. doi:10.1093/mnras/staa2491
- Raithel, C. A., Özel, F., & Psaltis, D. 2016, *PhRvC*, 93, 032801. doi:10.1103/PhysRevC.93.032801
- Read, J. S., Lackey, B. D., Owen, B. J., et al. 2009, *PhRvD*, 79, 124032. doi:10.1103/PhysRevD.79.124032
- Reed, B. T., Fattoyev, F. J., Horowitz, C. J., et al. 2021, *PhRvL*, 126, 172503.
doi:10.1103/PhysRevLett.126.172503
- Ribes, P., Ramos, A., Tolos, L., et al. 2019, *ApJ*, 883, 168.
doi:10.3847/1538-4357/ab3a93
- Rikovska Stone, J., Guichon, P. A. M., Matevosyan, H. H., et al. 2007, *NuPhA*, 792, 341.
doi:10.1016/j.nuclphysa.2007.05.011
- Riley, T. E., Watts, A. L., Bogdanov, S., et al. 2019, *ApJL*, 887, L21. doi:10.3847/2041-8213/ab481c
- Riley, T. E., Watts, A. L., Bogdanov, S., et al. 2019, v1.0.0, *Zenodo*, doi:10.5281/zenodo.3386449
- Riley, T. E., Watts, A. L., Ray, P. S., et al. 2021, *arXiv:2105.06980*
- Riley, T. E., Watts, A. L., Ray, P. S., et al. 2021, v1.0.0, *Zenodo*, doi:10.5281/zenodo.4697625
- Sen, D. & Jha, T. K. 2019, *Journal of Physics G Nuclear Physics*, 46, 015202. doi:10.1088/1361-6471/aaf0b0
- Silva, H. O., Holgado, A. M., Cárdenas-Avendaño, A., et al. 2021, *PhRvL*, 126, 181101.
doi:10.1103/PhysRevLett.126.181101
- Steiner, A. W., Gandolfi, S., Fattoyev, F. J., et al. 2015, *PhRvC*, 91, 015804. doi:10.1103/PhysRevC.91.015804
- Sun, B. Y., Liu, Z. W., & Xing, R. Y. 2019, *Xiamen-CUSTIPEN Workshop on the Equation of State of Dense Neutron-Rich Matter in the Era of Gravitational Wave Astronomy*, 2127, 020020. doi:10.1063/1.5117810

- Urbanec, M., Miller, J. C., & Stuchlík, Z. 2013, MNRAS, 433, 1903. doi:10.1093/mnras/stt858
- Wei, J.-B., Figura, A., Burgio, G. F., et al. 2019, Journal of Physics G Nuclear Physics, 46, 034001. doi:10.1088/1361-6471/aaf95c
- Worley, A., Krastev, P. G., & Li, B.-A. 2008, ApJ, 685, 390. doi:10.1086/589823
- Xie, W.-J. & Li, B.-A. 2021, PhRvC, 103, 035802. doi:10.1103/PhysRevC.103.035802
- Yagi, K. & Yunes, N. 2013, PhRvD, 88, 023009. doi:10.1103/PhysRevD.88.023009
- Yuan, Y. F. & Zhang, J. L. 1999, ApJ, 525, 950. doi:10.1086/307921
- Zhu, Z.-Y., Zhou, E.-P., & Li, A. 2018, ApJ, 862, 98. doi:10.3847/1538-4357/aacc28